Proceedings of the Twenty-sixth (2016) International Ocean and Polar Engineering Conference
Rhodes, Greece, June 26-July 1, 2016

ISBN 978-1-880653-88-3; ISSN 1098-6189

www.isope.org

Generation of Very Long Waves in Laboratory for Tsunamis Research

Heng Lu[1], Yong Sung Park[1], Yong-Sik Cho[2]

[1]School of Science and Engineering
University of Dundee
Dundee, United Kingdom

[2]Civil and Environmental Engineering
Hanyang University
Seoul, Korea

ABSTRACT

Over the last few decades, solitary waves have been commonly used as the model tsunami waves, but their wavelength-to-depth ratios are much smaller than that of tsunamis in reality. On the other hand, generating waves that are longer than solitary waves in laboratory is in fact a very challenging task. In this study, a new kind of wave maker is designed and investigated, which has a moving bottom at the toe of the beach as the wave generating mechanism with adjustable slope. By changing some characteristic parameters, different waves are generated and investigated theoretically and experimentally.

KEY WORDS: long waves; tsunami; finite volume method; linear wave theory; nonlinear effects; wave maker.

INTRODUCTION

Since the early 1970s, solitary wave has been the most commonly used tsunami wave model in theoretical and experimental studies of tsunamis (e.g., Synolakis, 1987; Liu et al., 1995; Li and Raichlen, 2002; Craig, 2006). It has been usually believed solitary wave can capture many main features of how tsunami waves behave in coastal region. Typical solitary wave expression as a solution to the KdV equation (e.g., Madsen and Schäffer, 2010) reads

$$\eta(x,t) = A_s \,\mathrm{sech}^2(K_s(x-ct)), \quad K_s = \frac{1}{h}\sqrt{\frac{3A_s}{4h}}, \tag{1}$$

where η, A_s, c and h denote free surface elevation, wave height, phase velocity and static water depth, respectively. Notice that wavenumber K_s is tied to amplitude-to-depth ratio A_s/h which is usually regarded as nonlinearity.

However, based on the definition of the wavenumber K_s, Madsen et al. (2008) questioned the link between solitary wave and geophysical tsunamis, and clarified their views that solitary wave is not appropriate to model important characteristics of tsunamis. First of all, because of the linear dispersion occurs in deep water, they suggested linear KdV equation to be used for wave generation. Secondly, along with tsunami waves approaching the beach, frequency dispersion will decrease while the nonlinearity will increase significantly, leading to skewness of waves, which is already beyond the KdV scale. Moreover, during wave breaking, some very short KdV waves in the front of the tsunami wave will break too early which can mislead people to make wrong investigation of the corresponding run-up. Therefore, Madsen et al. (2008) illustrated that the tie between the wavenumber K_s and the nonlinearity A_s/h in Eq. (1) is no longer realistic for geophysical tsunamis. In fact, full scale tsunami measurements confirmed the inadequacy of using solitary wave paradigm as well. In Fig. 1, the records of the 2011 Japan Tohoku tsunami clearly show that solitary wave is not long enough when compared to the observed leading tsunami wave with the same amplitude.

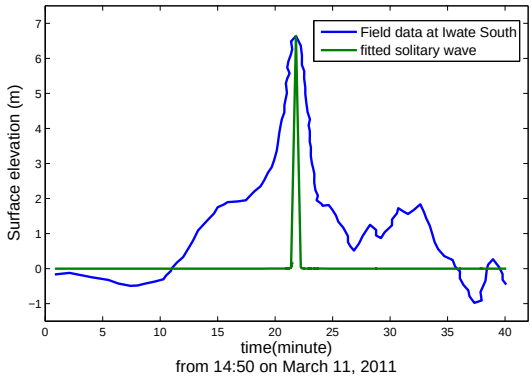

Fig. 1 : Comparison between field data at Iwate South from Japan Tohoku tsunami in 2011 (digitized from Chan and Liu (2012)) and fitted solitary wave.

For theoretical investigation, a variety of wave theories have been adopted to examine the wave behaviour. In early stage, people evaluated the wave motion from the linear theory in tsunami studies (e.g., Ka-

jiura, 1963; Keller and Keller, 1964; Tuck and Hwang, 1972; Synolakis, 1987). When nonlinearity makes significant influence, the classical nonlinear shallow water (NSW) equations have been usually employed for simulating waves:

$$\left.\begin{array}{l} \eta_t + ((h+\eta)u)_x + h_t = 0, \\ u_t + uu_x + g\eta_x = 0, \end{array}\right\} \tag{2}$$

where u denotes the depth-averaged fluid velocity and g is the gravitational acceleration. On the other hand, frequency dispersion is of great importance during wave generation and propagation when pressure cannot be assumed hydrostatic. Many studies have shown that dispersive models have good performances on long wave simulation (e.g., Peregrine, 1967; Zelt, 1991; Dutykh et al., 2011; Dutykh and Kalisch, 2013). In this work, the Boussinesq system derived by Wu (1987) for dynamic bathymetry is employed:

$$\left.\begin{array}{l} \eta_t + ((h+\eta)u)_x + h_t = 0, \\ u_t + g\eta_x + uu_x = \frac{1}{2}h(h_t + (hu)_x)_{xt} - \frac{1}{6}h^2 u_{xxt}. \end{array}\right\} \tag{3}$$

A wide range of numerical methods are developed in solving these hyperbolic equations, such as finite difference methods, finite element methods, finite volume methods and discontinuous Galerkin methods. Finite volume scheme is used in the study as it is good at approximating solutions to conservative equations with high efficiency, accuracy and robustness owing to its conservative and shock-capturing properties (Dutykh and Kalisch, 2013). Since how to deal with the discontinuity of discrete solution at the cell interfaces is of key importance, Dutykh et al. (2011) introduced three types of numerical fluxes which can take effect along with some reconstruction techniques such as TVD (Sweby, 1984), UNO (Harten and Osher, 1987) and WENO (Liu et al., 1994) schemes. Among the three types, a Lax-Friedrichs type flux, is chosen in this work. For reconstruction techniques, either UNO2 scheme (Harten and Osher, 1987) or WENO scheme (such as WENO3 and WENO5) uses adaptive stencil to interpolate the numerical flux and keep the piecewise polynomial representations always non-oscillatory.

As in theoretical studies, solitary wave has been the popular one for being a tsunami wave model for experiments. Indeed one of the reasons that solitary waves have been so popular for such a long time was that they are relatively easy to generate in the laboratory(Goring, 1978). In a typical laboratory wave tank, a piston-type wave maker is widely used to generate long waves. It generates approximately uniform flow field in the vertical direction, which is an important characteristic of long waves. However, those traditional piston-type wave makers are limited in their stroke lengths. Additionally, a wave longer than the corresponding solitary wave for the same wave height will disintegrate into shorter ones (a series of solitary waves) due to dispersion by the time they arrive at the other end of the tank. Among these relevant experimental studies, very few of them mentioned using bottom-wave-generator to simulate tsunami generation or create long waves. The well known one is the bottom-wave-generator designed by Hammack (1973) for modelling tsunami waves excited by vertical bottom motion in an ocean of uniform depth.

Based on the query of if solitary wave is able to represent the geophysical scales of tsunamis by Madsen et al. (2008) and the comparison between field observation and relevant solitary waves, generating waves that are longer than solitary waves in laboratory worths attracting our attention. But it has been left as a void in tsunami studies. In the present study, a new wave maker is used to generate waves with relatively large wavelength-to-depth ratio and small wave height-to-depth ratio. By moving the entire bottom, the length of the wave generated would be as long as that of the tank itself, which should be the longest wave in any given tank. A sketch of the bottom-tilting wave maker is depicted in Fig. 2, and the wave maker will be introduced in detail in the later section.

The present study introduces linear wave theory and weakly nonlinear and weakly dispersive wave theory in the following first two sections. Then the experiments are introduced. Based on the theoretical and experimental results, we can verify the resulting long waves by comparing them with the corresponding solitary waves with same amplitude. Additionally, the effects of the motion amplitude and speed of the bottom motion of the wave maker on the resulting waves are further discussed and concluded in the last two sections.

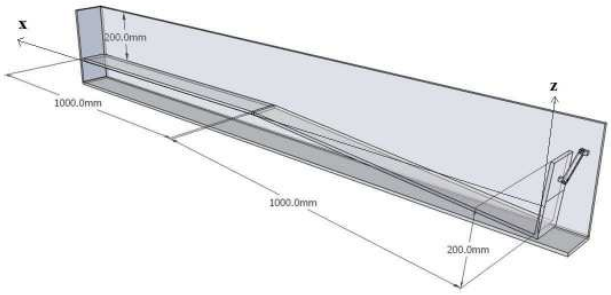

Fig. 2 : Sketch of the bottom-tilting wave maker.

LINEAR WAVE THEORY

For theoretical investigation of long wave generation, the potential-flow free surface problem governs the motion of the fluid under the assumptions of being inviscid, incompressible and irrotational flow in this study. In addition, bottom dissipation is ignored and full reflection happens at the tank ends. As shown in Fig. 2, the analysis is divided into two parts by the toe of the slope. The moving bottom part will generate long waves, and the other part is for the generated waves propagating in the constant water depth. The coordinate system origins at the end wall of the generation part, meanwhile the positive x axis is pointing the other end wall and z axis is pointing upwards. Thus, the fluid domain is bounded by the two end walls, the free surface and the bottom solid boundary, while the latter two are defined as $z = \eta(x,t)$ on the surface and $z = -h(x,t)$ at the bottom, where η denotes the surface elevation and h the water depth. For $0 < x < L$, water depth $h(x,t) = h_0 - \zeta(x,t)$, where ζ denotes the bottom motion displacement, L the moving bottom length, and h_0 the initial water depth.

Linear wave theory enables to quickly estimate the generated waves but with the limitation that it only applies to non-breaking waves and where nonlinear effects are small. With Φ denoting the velocity potential, continuity equation reads:

$$\nabla^2\Phi = \frac{\partial^2\Phi}{\partial x^2} + \frac{\partial^2\Phi}{\partial z^2} = 0, \tag{4}$$

with boundary conditions introduced from the linearized kinematic and dynamic boundary conditions

$$\frac{\partial\eta}{\partial t} = \frac{\partial\Phi}{\partial z}, \quad z = 0, \tag{5}$$

$$\frac{\partial\Phi}{\partial t} + g\eta = 0, \quad z = 0, \tag{6}$$

$$\frac{\partial\Phi}{\partial z} = \frac{\partial\zeta}{\partial t} \equiv W(x,t), \quad z \cong -h_0. \tag{7}$$

When the Laplace transform in t (denoted by $\bar{}$) and Fourier transform in x (denoted by $\tilde{}$) are applied as Mei (1989) suggested, the equations read

$$\frac{d^2\tilde{\bar{\Phi}}}{dz^2} - k^2\tilde{\bar{\Phi}} = 0, \quad -h_0 \le z \le 0, \tag{8}$$

$$\frac{d\tilde{\bar{\Phi}}}{dz} + \frac{s^2}{g}\tilde{\bar{\Phi}} = 0, \quad z = 0, \tag{9}$$

$$\frac{\partial\tilde{\bar{\Phi}}}{\partial z} = \tilde{\bar{W}}, \quad z = -h_0, \tag{10}$$

while the velocity potential is now given in the form

$$\Phi(x,z,t) = \frac{1}{2\pi}\int_{-\infty}^{\infty} dk\, e^{ikx}\frac{1}{2\pi i}\int_{\Gamma} ds\, e^{st}\tilde{\bar{\Phi}}(k,z,s). \tag{11}$$

Thus, the solution to the transformed velocity potential here is presented by

$$\tilde{\bar{\Phi}} = \frac{\tilde{\bar{W}}(s^2\sinh kz - gk\cosh kz)}{k(s^2+\omega^2)\cosh kh_0}, \tag{12}$$

where $\omega^2 = gk\tanh kh_0$ and k denotes wavenumber. Then, by substituting Eq. (11) into Eq. (5), the surface elevation becomes

$$\eta(x,t) = \frac{1}{2\pi}\int_{-\infty}^{\infty} dk\,\frac{e^{ikx}}{\cosh kh}\frac{1}{2\pi i}\int_{\Gamma} ds\,\frac{s\tilde{\bar{W}}e^{st}}{s^2+\omega^2}. \tag{13}$$

Due to the generating mechanism of this wave maker, the bottom will rotate around the hinge as the center and symmetrically at $x = 0$. The bottom motion displacement is given by

$$\zeta(x,t) = D_0(x)\,T(t), \tag{14}$$

where

$$D_0(x) = \begin{cases} a - \frac{a}{L}|x|, & -L \le x \le L, \\ 0, & x < -L \quad \text{and} \quad x > L. \end{cases} \tag{15}$$

Thus, from Eq. (7), it becomes

$$\frac{\partial\Phi}{\partial z} = \frac{\partial\zeta}{\partial t} = D_0(x)\,Q(t) = W(x,t), \tag{16}$$

where

$$T'(t) = Q(t). \tag{17}$$

According to the linear solution, substituting the Fourier transformed result of $D_0(x)$:

$$\tilde{D}_0(k) = 2\mathrm{Re}\int_0^{\infty} D_0(x)\,e^{-ikx}dx = aL\frac{\sin^2(kL/2)}{(kL/2)^2}, \tag{18}$$

into Eq. (13) gives the free surface elevation at the hinge

$$\eta(L,t) = \frac{aL}{\pi}\int_0^t du\int_0^{\infty} dk\,\frac{\sin^2(kL/2)}{(kL/2)^2}\frac{\cos kL}{\cosh kh}Q(u)\cos\omega(t-u). \tag{19}$$

As the bottom can move vertically upwards or downwards, these two basic types of motion are investigated in the present study. For upwards motion with constant velocity, velocity $Q(t)$ is defined as

$$Q(t) = \begin{cases} \frac{1}{b}, & 0 \le t \le b, \\ 0, & t \ge b, \end{cases} \tag{20}$$

hence the free surface elevation at the hinge becomes

$$\eta(L,t) = \begin{cases} \frac{aL}{\pi}\int_0^t du\int_0^{\infty} dk\,\frac{1}{b}\frac{\sin^2(kL/2)}{(kL/2)^2}\frac{\cos kL}{\cosh kh}\cos\omega(t-u), & 0 \le t \le b, \\ \frac{aL}{\pi}\int_0^b du\int_0^{\infty} dk\,\frac{1}{b}\frac{\sin^2(kL/2)}{(kL/2)^2}\frac{\cos kL}{\cosh kh}\cos\omega(t-u), & t \ge b. \end{cases} \tag{21}$$

For downwards motion with constant velocity, velocity $Q(t)$ is defined as

$$Q(t) = \begin{cases} -\frac{1}{b}, & 0 \le t \le b, \\ 0, & t \ge b, \end{cases} \tag{22}$$

leading to the free surface elevation at the hinge

$$\eta(L,t) = \begin{cases} -\frac{aL}{\pi}\int_0^t du\int_0^{\infty} dk\,\frac{1}{b}\frac{\sin^2(kL/2)}{(kL/2)^2}\frac{\cos kL}{\cosh kh}\cos\omega(t-u), & 0 \le t \le b, \\ -\frac{aL}{\pi}\int_0^b du\int_0^{\infty} dk\,\frac{1}{b}\frac{\sin^2(kL/2)}{(kL/2)^2}\frac{\cos kL}{\cosh kh}\cos\omega(t-u), & t \ge b. \end{cases} \tag{23}$$

NUMERICAL MODEL IN CONSIDERATION OF NONLINEARITY AND DISPERSION

Since the nonlinear effects are not small in the whole tank owing to the relatively shallow water, linear wave theory cannot describe the resulting waves accurately if all the nonlinear effects are ignored. Therefore, using Boussinesq equations is a good choice to demonstrate the wave generation as both weak dispersion and weak nonlinearity are included. After normalisation with the following dimensionless variables:

$$x^* = \frac{x}{h_0},\ h^* = \frac{h}{h_0},\ \eta^* = \frac{x}{h_0},\ t^* = t\sqrt{\frac{g}{h_0}}, \tag{24}$$

the Boussinesq equations Eq. (3) are rewritten as below

$$\left.\begin{array}{l} H_t + [Hu]_x = 0, \\ u_t + [\frac{1}{2}u^2 + (H-h)]_x = \frac{1}{2}hh_{xtt} + \frac{1}{2}h(hu)_{xxt} - \frac{1}{6}h^2u_{xxt}, \end{array}\right\} \tag{25}$$

where $H = \eta + h$, and asterisk denoting non-dimensionality is dropped from now on.

In order to conform to the conservation law and follow the finite volume scheme by Dutykh et al. (2011), Eq. (25) are rearranged in the form as below

$$\mathbf{V}_t + [\mathbb{F}(\mathbf{V})]_x = \mathbb{S}_b + \mathbb{M}(\mathbf{V}), \tag{26}$$

where the variable $\mathbf{V}$, the advective flux $\mathbb{F}(\mathbf{V})$, the source term $\mathbb{S}_b$ and the dispersive term $\mathbb{M}(\mathbf{V})$ are denoted respectively by $\mathbf{V} = \begin{pmatrix} H \\ u \end{pmatrix}$, $\mathbb{F}(\mathbf{V}) = \begin{pmatrix} Hu \\ \frac{1}{2}u^2 + (H-h) \end{pmatrix}$, $\mathbb{S}_b = \begin{pmatrix} 0 \\ \frac{1}{2}hh_{xtt} \end{pmatrix}$, $\mathbb{M}(\mathbf{V}) = \begin{pmatrix} 0 \\ \frac{1}{2}h(hu)_{xxt} - \frac{1}{6}h^2u_{xxt} \end{pmatrix}$.

By using the finite volume discretization, we can divide a real line $\mathbb{R}$ uniformly into cells $C_i = [x_{i-\frac{1}{2}}, x_{i+\frac{1}{2}}]$ with centers $x_i = \frac{1}{2}(x_{i-\frac{1}{2}} + x_{i+\frac{1}{2}})$ $(i \in \mathbb{Z})$ while Δx_i regarded as the length of the cell.

However, in terms of the nonlinear shallow water system, it can be derived from Eq. (26) without the dispersive term

$$\frac{d\bar{\mathbf{V}}}{dt} + \frac{1}{\Delta x}\left[\mathbb{F}\left(\mathbf{V}\left(x_{i+\frac{1}{2}},t\right)\right) - \mathbb{F}\left(\mathbf{V}\left(x_{i-\frac{1}{2}},t\right)\right)\right] = \frac{1}{\Delta x}\int_{C_i}\mathbf{S}_b(\mathbf{V})\,dx \equiv \bar{\mathbb{S}}_i, \tag{27}$$

where $\bar{\mathbf{V}}_i(t) = \frac{1}{\Delta x}\int_{C_i}\mathbf{V}(x,t)dx$ is regarded as cell average. Hence, the numerical scheme for nonlinear shallow water system is discussed firstly.

To deal with the discontinuity at cell interfaces in the discrete solution, numerical flux functions are replaced at the cell interfaces by

$$\mathbb{F}\left(\mathbf{V}(x_{i\pm\frac{1}{2}},t)\right) \approx \mathbb{F}_{i\pm\frac{1}{2}}\left(\bar{\mathbf{V}}^{L}_{i\pm\frac{1}{2}},\bar{\mathbf{V}}^{R}_{i\pm\frac{1}{2}}\right), \tag{28}$$

where $\bar{\mathbf{V}}^{L,R}_{i\pm\frac{1}{2}}$ represents the reconstructions of the conservative variables $\bar{\mathbf{V}}$ from left and right sides of each cell interface. Hence, the semi-discrete scheme Eq. (27) becomes

$$\frac{d\bar{\mathbf{V}}_i}{dt} + \frac{1}{\Delta x}\left[\mathbb{F}_{i+\frac{1}{2}} - \mathbb{F}_{i-\frac{1}{2}}\right] = \bar{\mathbb{S}}_i. \tag{29}$$

Moreover, Lax-Friedrichs numerical flux function is used for $\mathbb{F}$:

$$\mathcal{F}(\mathbf{V},\mathbf{W}) = \frac{1}{2}\left\{[\mathbb{F}(\mathbf{W}) + \mathbb{F}(\mathbf{V})] - \mathbb{U}(\mathbf{V},\mathbf{W})[\mathbf{W}-\mathbf{V}]\right\}. \tag{30}$$

And the operator $\mathbb{U}$ is defined as

$$\mathbb{U}(\mathbf{V},\mathbf{W}) = \max[\rho(DF(\mathbf{V})),\rho(DF(\mathbf{W}))], \tag{31}$$

where DF denotes the Jacobian matrix and $\rho(I)$ is the spectral radius of I.

For the purpose of achieving higher order approximations to $\mathbf{V}(x_{i+\frac{1}{2}},t)$, some reconstruction methods of higher order accuracy aforementioned are employed.

UNO

Here, a piecewise polynomial representation called UNO2 is introduced which has a good performance as being of second order accuracy and results in small dissipation in wave computation. Following Dutykh et al. (2011)'s instruction, $\mathbf{V}^{L}_{i+\frac{1}{2}}$, $\mathbf{V}^{R}_{i+\frac{1}{2}}$ are respectively defined by

$$\mathbf{V}^{L}_{i+\frac{1}{2}} = \mathbf{V}_i + \frac{1}{2}\mathbf{S}_i, \quad \mathbf{V}^{R}_{i+\frac{1}{2}} = \mathbf{V}_{i+1} - \frac{1}{2}\mathbf{S}_i, \tag{32}$$

where

$$\mathbf{S}_i = m(\mathbf{S}_i^{+},\mathbf{S}_i^{-}), \quad \mathbf{S}_i^{\pm} = \delta_{i\pm\frac{1}{2}}\mathbf{V} \mp \frac{1}{2}\mathcal{D}_{i\pm\frac{1}{2}}\mathbf{V},$$
$$\delta_{i\pm\frac{1}{2}}\mathbf{V} = \mathbf{V}_{i+1} - \mathbf{V}_i, \quad \mathcal{D}_{i\pm\frac{1}{2}}\mathbf{V} = m(\mathcal{D}_i\mathbf{V},\mathcal{D}_{i+1}\mathbf{V}),$$
$$\mathcal{D}_i\mathbf{V} = \mathbf{V}_{i+1} - 2\mathbf{V}_i + \mathbf{V}_{i-1}, \quad m(x,y) = \frac{1}{2}(\mathrm{sign}(x)+\mathrm{sign}(y))\min(|x|,|y|),$$

and $m(x,y)$ denotes the minmod function as a limiter in UNO2 scheme.

WENO

WENO type reconstruction can lead to higher order accuracy, for example, 3rd order accurate WENO3 and 5th order accurate WENO5. Here just WENO3 scheme is introduced for simplicity, while WENO5 scheme can be also found in Shu (1998).

First order reconstructed values are defined as

$$\left.\begin{array}{ll} \mathbf{V}^{(0)}_{i+\frac{1}{2}} = \frac{1}{2}(\mathbf{V}_i + \mathbf{V}_{i+1}), & \mathbf{V}^{(1)}_{i+\frac{1}{2}} = \frac{1}{2}(-\mathbf{V}_{i-1} + 3\mathbf{V}_i), \\ \mathbf{V}^{(0)}_{i-\frac{1}{2}} = \frac{1}{2}(3\mathbf{V}_i - \mathbf{V}_{i+1}), & \mathbf{V}^{(1)}_{i-\frac{1}{2}} = \frac{1}{2}(\mathbf{V}_{i-1} + \mathbf{V}_i). \end{array}\right\} \tag{33}$$

Then, the smoothness parameters are defined as

$$\beta_0 = (\mathbf{V}_{i+1} - \mathbf{V}_i)^2, \quad \beta_1 = (\mathbf{V}_i - \mathbf{V}_{i-1})^2, \tag{34}$$

and the other parameters are defined as $d_0 = \frac{2}{3}$, $d_1 = \frac{1}{3}$ and $\tilde{d}_0 = d_1$, $\tilde{d}_1 = d_0$, along with the weights

$$\omega_0 = \frac{\alpha_0}{\alpha_0+\alpha_1}, \omega_1 = \frac{\alpha_1}{\alpha_0+\alpha_1}, \tilde{\omega}_0 = \frac{\tilde{\alpha}_0}{\tilde{\alpha}_0+\tilde{\alpha}_1}, \tilde{\omega}_1 = \frac{\tilde{\alpha}_1}{\tilde{\alpha}_0+\tilde{\alpha}_1}, \tag{35}$$

where $\alpha_i = \frac{d_i}{\epsilon+\beta_i}$, $\tilde{\alpha}_i = \frac{\tilde{d}_i}{\epsilon+\beta_i}$ with ϵ being a small and positive number. Finally, the reconstructed values are given by

$$\mathbf{V}^{L}_{i+\frac{1}{2}} = \sum \omega_r \mathbf{V}^{(r)}_{i+\frac{1}{2}}, \quad \mathbf{V}^{R}_{i-\frac{1}{2}} = \sum \omega_r \mathbf{V}^{(r)}_{i-\frac{1}{2}}. \tag{36}$$

As the discretization should keep well balanced and preserve the upwind nature, Dutykh et al. (2011) suggested the source terms to be:

$$\frac{1}{\Delta x}\int_{c_i}\mathbb{S}_b(\mathbf{V})dx \approx \frac{\mathbb{S}_{b\,i-\frac{1}{2}} + \mathbb{S}_{b\,i+\frac{1}{2}}}{2}, \quad \mathbb{S}_{b\,i+\frac{1}{2}} = \mathbb{S}_b\left(\frac{\mathbf{V}^{L}_{i+\frac{1}{2}} + \mathbf{V}^{R}_{i+\frac{1}{2}}}{2}\right). \tag{37}$$

So far, the numerical scheme for nonlinear shallow water system has been built. However, dispersive terms are left to be dealt with if Boussinesq equations are expected to be solved. Additionally, for keeping dispersive terms approximation of the same order as the UNO2 reconstructed flux discretization, the dispersive terms are discretized by

$$\begin{aligned} \mathbf{M}_i(\bar{\mathbf{V}}) &= \frac{1}{2}\bar{h}_i\frac{\bar{h}_{i+1}(\bar{u}_t)_{i+1} - 2\bar{h}_i(\bar{u}_t)_i + \bar{h}_{i-1}(\bar{u}_t)_{i-1}}{\Delta x^2} \\ &\quad - \frac{1}{6}\bar{h}_i^2\frac{(\bar{u}_t)_{i+1} - 2(\bar{u}_t)_i + (\bar{u}_t)_{i-1}}{\Delta x^2} \\ &= \frac{\bar{h}_i}{2\Delta x^2}(\bar{h}_{i-1} - \frac{1}{3}\bar{h}_i)(\bar{u}_t)_{i-1} \\ &\quad - \frac{2}{3\Delta x^2}\bar{h}_i^2(\bar{u}_t)_i + \frac{\bar{h}_i}{2\Delta x^2}(\bar{h}_{i+1} - \frac{1}{3}\bar{h}_i)(\bar{u}_t)_{i+1}, \end{aligned} \tag{38}$$

which is of the second order accuracy as well (Dutykh and Kalisch, 2013). Thus, the semi-discrete scheme for Boussinesq equations can be rewritten as

$$\left.\begin{array}{l} \frac{d\bar{H}}{dt} + \frac{1}{\Delta x}[\mathbb{F}^{(1)}_{+}(\bar{\mathbf{V}}) - \mathbb{F}^{(1)}_{-}(\bar{\mathbf{V}})] = 0 \\ (I-M)\cdot\frac{d\bar{u}}{dt} + \frac{1}{\Delta x}[\mathbb{F}^{(2)}_{+}(\bar{\mathbf{V}}) - \mathbb{F}^{(2)}_{-}(\bar{\mathbf{V}})] = \mathbb{S}^{(2)}_{b}, \end{array}\right\} \tag{39}$$

where $\mathbb{F}^{(1,2)}_{\pm}(\bar{\mathbf{V}})$ are the two components of the flux vector $\mathbb{F}$ at the right (+) and left (-) faces respectively, and $\mathbb{S}^{(2)}_b$ is the second component of the source term vector $\mathbb{S}_b$. Moreover, Dutykh et al. (2011)confirmed that this second order central difference scheme can ensure WENO3 scheme of a global second order accuracy. Li and Raichlen (2002) combined the similar dispersive terms discretization with their numerical scheme for nonlinear shallow water equations where WENO5 scheme was used as the reconstruction method and verified their numerical model by simulating solitary wave propagation.

Time discretization used here is a Runge-Kutta scheme of the third order with three stages proposed by Bogacki and Shampine (1989):

$$\begin{aligned} k_1 &= \mathcal{N}(\mathbf{V}^n, t_n), \\ k_2 &= \mathcal{N}(\mathbf{V}^n + \tfrac{1}{2}\Delta t k_1, t_n + \tfrac{1}{2}\Delta t), \\ k_3 &= \mathcal{N}(\mathbf{V}^n + \tfrac{3}{4}\Delta t k_2, t_n + \tfrac{3}{4}\Delta t), \\ \mathbf{V}^{n+1} &= \mathbf{V}^n + \Delta t(\tfrac{2}{9}k_1 + \tfrac{1}{3}k_2 + \tfrac{4}{9}k_3). \end{aligned} \tag{40}$$

Owing to the two solid walls at the two tank ends respectively, the boundary conditions are determined as totally reflective. Hence, the wave velocity at the wall is imposed to be zero. In addition, ghost cells are added to the boundaries depending on different numerical schemes with the three different reconstruction methods introduced. According to the finite volume discretization, the imposed boundary conditions are described

$$\left.\begin{array}{l} H_0 = H_1, \\ (u)_0 = -(u)_1, \\ (u)_{\frac{1}{2}} = 0, \end{array}\right\} \tag{41}$$

where the index 0 indicates the ghost cell.

The computational domain was discretized with $\delta x = 1/3$, and $\delta t = 0.1$ for computational efficiency and stability. The Courant-Friedrichs-Lewd (CFL) condition, which demonstrates the variants cannot run faster and skip any cell in a single time step, has been verified and satisfied with this discretization. For the equation system (26), the propagation speed is determined by the eigenvalues of the flux Jacobian matrix, where the flux Jacobian matrix is given by

$$\frac{\partial \mathbb{F}(\mathbf{V})}{\partial \mathbf{V}} = \begin{pmatrix} u & H \\ 1 & u \end{pmatrix} \tag{42}$$

and it leads to two eigenvalues defined as

$$\lambda^{\pm} = u \pm c_s, \quad c_s \equiv \sqrt{H}. \tag{43}$$

Therefore, the propagation speed λ cannot exceed the cell speed $\frac{dx}{dt}$, which can be used to define the Courant number as shown below

$$C_r = \frac{dt}{dx} \max(|\lambda|) \tag{44}$$

and to ensure $C_r < 1$ all the time to satisfy the CFL condition. With this discretization, C_r is less than 0.5 at each time step.

A solitary wave in constant-depth water is used to validate this finite volume scheme if the wave will always keep its shape during its propagation. The exact solution to solitary wave $\eta = A\,\mathrm{sech}^2(\frac{3A}{4h^3})^{1/2}(x-3.5L_s)$ at $t = 0$ is used as the initial condition. Also, $\mathbb{S}_b = \mathbf{0}$ is used for constant depth. Fig. 3 displays the solitary waves solved by UNO2, WENO3 and WENO5 with second order dispersive terms separatively. The three numerical methods all closely approximate the exact solution. For making it a well balanced numerical method, Dutykh et al. (2011) suggested that WENO scheme should better be combined with higher order scheme for the dispersive terms due to its higher order of accuracy. Hence, only UNO2 scheme is decided to be used for solving Boussinesq equations, while WENO scheme is used for solving NSW equations as no dispersive terms considered for the following investigations.

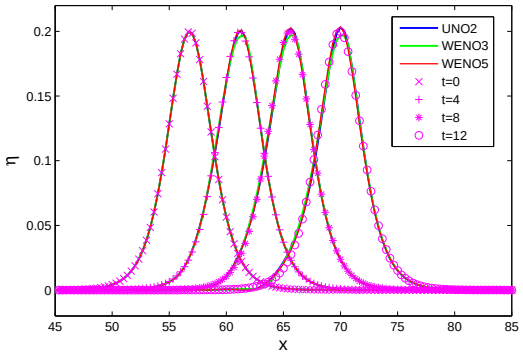

Fig. 3 : Comparisons of solitary wave between the three schemes (solid lines are distinguished by colour as marked) and the exact solution (magenta symbols).

EXPERIMENTS

A series of experiments were carried out in the wave tank which consists of an adjustable slope and wave generator. The moving bottom is 1 m long and 0.11 m wide. The hinge is located at which the depth is 0.2 m from the top of the tank. The tank is 2.185 m long, 0.11 m wide and 0.3 m deep, which leaves enough space for varying bottom motions. The programmable wave generator is located at the right end of the tank driven by an electrical servo motor. The expected bottom motion was programmed and implemented within a wide range of speeds and maximum displacement within 0.1 m. Rubber seal and membrane were attached around the moving bottom to ensure impermeability. The wheel on the right leg of the tank was used for adjusting the slope of the fixed bed. Hence, the beach with desired slope was created since the left bottom is fixed to the tank. However, the fixed bottom was always flat with no slope in the present study focusing on wave generation. Adjustable slope can be used for future investigation.

Two acoustic wave gauges were used to measure the free surface elevation at hinge (x=1 m) and middle of the fixed bottom (x=1.5 m) respectively. The two wave gauges are ultrasonic sensors with analog output relying on varying voltage with time proportional to time history of displacement, while the ultrasonic frequency is 300 kHz with the time resolution of being 30 ms. Both wave gauges were located at least 0.1 m above the water surface since the wave gauge has a sensing range of 0.03 m to 0.3 m. The two acoustic wave gauges were calibrated separately by measuring some different distances before the experiments in order to convert the electrical signal into the real displacement precisely, accompanying the tolerant error of the ultrasonic sensor as ±0.5 mm in this mode. For the experiments, the measurement frequency was set to be 50 Hz and measurement duration time was 10 seconds which begins with the bottom motion, and is sufficient to measure the time history of free surface elevation.

Due to the symmetry of the discussed bottom motion aforementioned, the origin of the physical model was represented by the intersection point between the right end wall and the flat moving-bottom, and only half of the motion was modelled. In the present study, only linear vertical motions with constant speed were considered as described by Eq. (15). Thus, the characteristic parameters of the bottom motion, i.e. displacement a and motion duration time b, were required and can be easily used to control the bottom motion. Bottom motion displacement ranged from 0.5 to 4 cm, which provided the scaled motion amplitude a/h_0 ranging from 0.083 to 1.0, with the three water depths being 4 cm, 5 cm and 6 cm. Hence, the disturbance size scales L/h_0 yielded from 16.7 to 25. Meanwhile, bottom motion duration time ranged from 0.5 to 2 s.

RESULTS

As aforementioned, simple linear upwards and downwards motions are used as the basic motions in this study. Once a bottom motion is introduced into the system, Boussinesq equations (25) are solved numerically or the solution to Eq. (23) of the free surface elevation at hinge is acquired according to the linear wave theory. The varying water depths, bottom motion displacements and durations for a series of experiments are shown in Table 1. Fig. 4 shows the comparison of time history of the free surface elevation at hinge between experimental data and theoretical results, where (a) shows the waves generated by upwards motion and (b) downwards motion.

Obviously, the numerical model based on Boussinesq equations can closely approximate the waves generated by the new wave maker. The numerical results by solving nonlinear shallow water equations show good agreement with the experimental data as well, but cannot simulate the dispersion in the generation region. Therefore, Boussinesq equations

have better performance than nonlinear shallow water equations for wave generation.

Table 1 : Parameters for varying bottom motions.

Parameters	Values
Water depth h_0 (m)	0.060, 0.050, 0.040
Bottom motion displacement a (m)	0.005, 0.010 $\cdots$ 0.040
Bottom motion duration b (s)	0.5, 1.0, 1.5, 2.0

However, due to the reflection in the wave tank, it is difficult to compare the first order wave directly from Fig. 4. In the meanwhile, the analytical solution to Eq. (23) by the linear theory is not able to approximate the waves in the tank because of reflection. The analytical solution is to quickly predict the first order wave generated by this wave maker in infinite long tank. Thus, the wave tank is assumed to be long enough for a complete leading wave obtained at hinge theoretically. Additionally, the analytical solution is used as a basis to define the amplitude and position of the comparative solitary wave. Then, the theoretical results are compared with the corresponding solitary waves, which are shown in Fig. 5 for upwards motion and Fig. 6 for downwards motion, respectively. Clearly, the comparison demonstrates that the waves created by the bottom tilting wave maker are much longer than the corresponding solitary waves with same wave amplitude. Moreover, the differences between numerical results and analytical solution indicate the importance of nonlinear effects even in wave generation region. Note that reflection can be controlled theoretically by inversely Fourier transforming the reflected waves to obtain the corresponding bottom motion. The opposite bottom motion will be applied to the tank in laboratory to absorb the unwanted waves in future studies.

ANALYSIS

Based on Table 1, different waves are generated and investigated. Wave amplitude and wave period of the resulting waves are the main features to be examined for wave generation. The influences of varying bottom motion displacement a and duration time b on the amplitudes and periods of the resulting leading waves are respectively shown in Fig. 7 for upwards motion and Fig. 8 for downwards motion with water depth of 0.05 m. The figures indicate that greater bottom motion duration time b leads to decreasing amplitude A but increasing period T of the waves for both upwards and downwards motions. In the meanwhile, greater bottom motion displacement a results in greater wave amplitude A. However, wave period T decreases with growing bottom displacement a for upwards motion but increases with increasing bottom displacement a for downwards motion. Similar results were observed in cases with the other two water depths.

Besides, bottom displacement a does not affect the wave period T obtained from the analytical solution, which is physically correct for the linear theory. In other words, the bottom motion displacement has more noticeable influences on wave amplitude than wave period from the linear theory. Obviously, the duration of the bottom motion affects both of amplitude and period of the wave. Due to the difference between linear wave theory and the numerical models in terms of nonlinearity, it is confirmed again that nonlinear effects are not negligible and better taken into consideration for wave generation region.

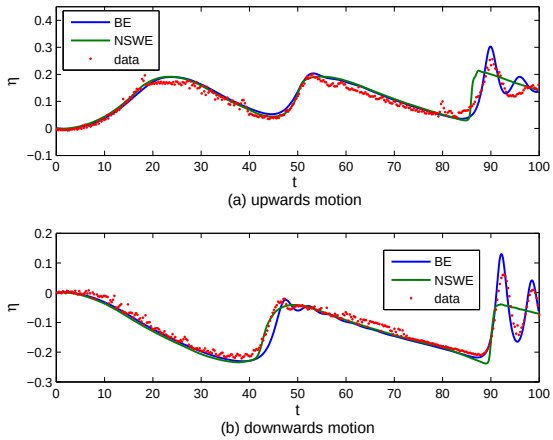

Fig. 4 : Comparison of free surface elevation at hinge (BE: Boussinesq equations, NSWE: nonlinear shallow water equations).

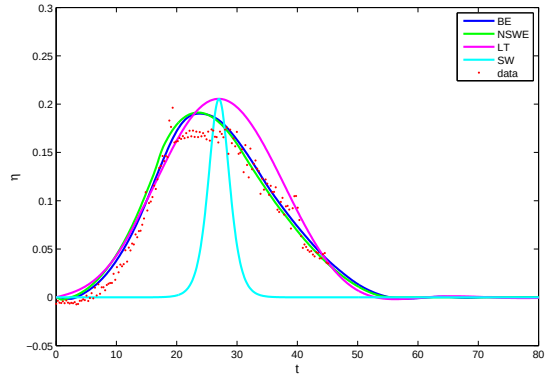

Fig. 5 : Comparison of first order wave at hinge for upwards motion (LT: linear theory, SW: solitary wave).

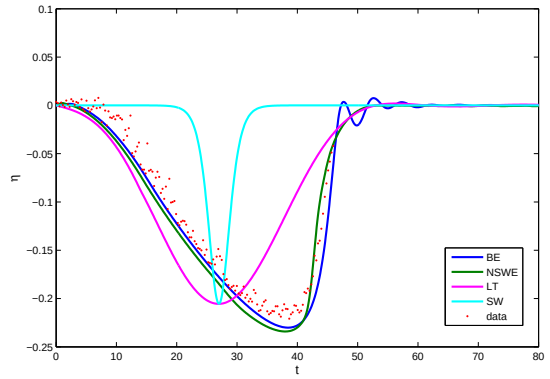

Fig. 6 : Comparison of first order wave at hinge for downwards motion.

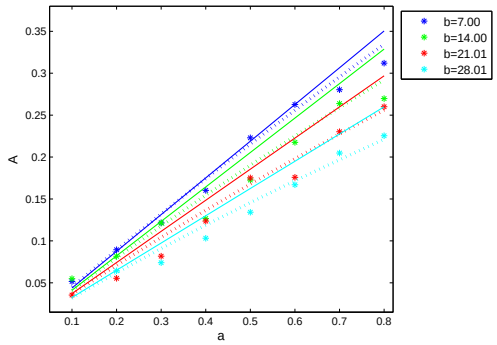

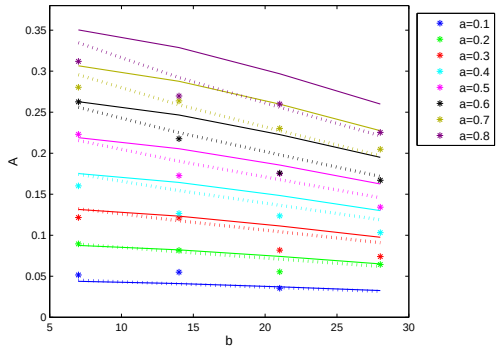

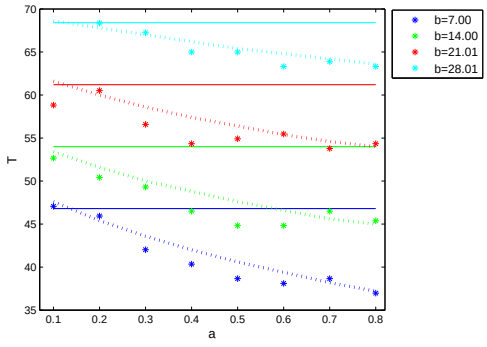

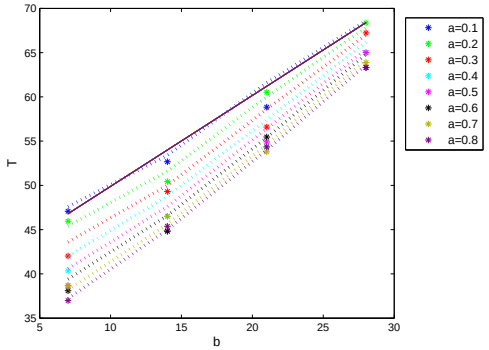

Fig. 7 : Effects of bottom motion on amplitude and period of the resulting wave for upwards motion (solid line indicates results by linear wave theory, dotted line indicates results from Boussinesq equations, asterisk indicates measurement, while *a* and *b* are distinguished by colour as marked).

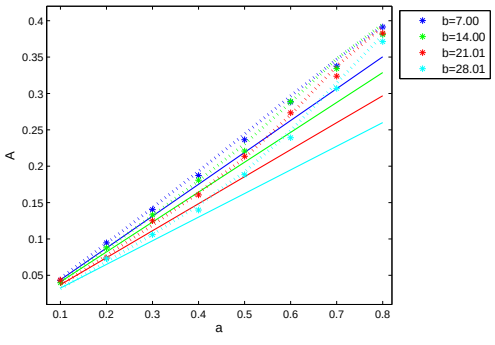

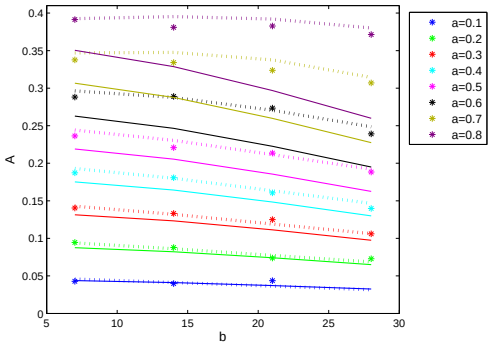

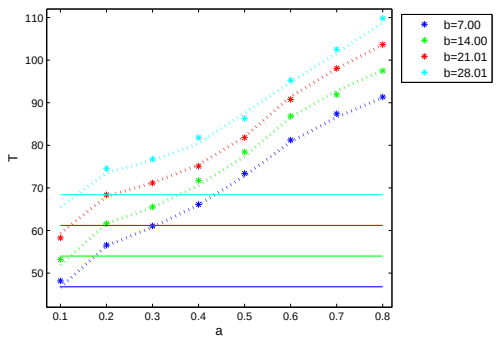

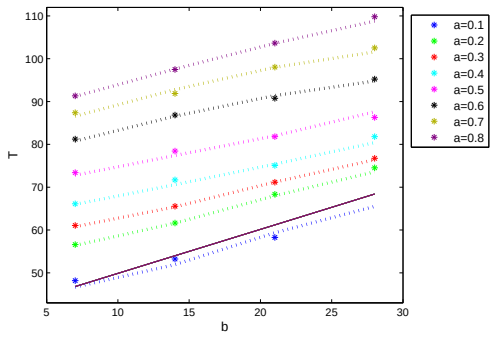

Fig. 8 : Effects of bottom motion on amplitude and period of the resulting wave for downwards motion (solid line indicates results by linear wave theory, dotted line indicates results from Boussinesq equations, asterisk indicates measurement, while *a* and *b* are distinguished by colour as marked).

CONCLUSIONS

Recently questions have been raised on using solitary waves in tsunamis research as the wavelength-to-depth ratio of the solitary waves are several orders-of-magnitude smaller than that of the tsunamis in reality. Therefore it is important to generate truly long waves in the laboratory for further research in this area. The new wave generator used in this study is a bottom-tilting wave maker, which makes long waves by moving the bottom hinged at the toe of the beach with adjustable slope under the command of an electric servo motor.

Theoretically, the linear wave theory can be used to provide the time history of the water surface elevation at the toe of the beach. Furthermore, in terms of the influence of nonlinearity, we have built a numerical model based on the weakly nonlinear and weakly dispersive wave theory. The theoretical results have been compared with the experimental measurements, which confirms that the new wave maker can truly generate longer waves than the corresponding solitary waves with the same wave amplitude. Moreover, according to the comparison between the analytical solutions from the linear wave theory and the numerical results from equations in consideration of nonlinearity solved by finite volume method, it should be noted that nonlinear effects are important and necessary to be taken into consideration for practically modelling the waves generated by this new wave maker. Moreover, including dispersion in the numerical model is helpful in simulating higher order waves more accurately. As a result, surface waves studied in Boussinesq scaling with time-dependent bottom bathymetry gives a better performance.

The waves generated by the wave maker are investigated mainly on the wave amplitude and wave period for the wave generation. By changing water depth, bottom motion displacement and speed, different waves are created and investigated. The resulting wave amplitude increases with either increasing bottom motion displacement or decreasing motion duration time. Meanwhile, the resulting wave period increases with growing bottom motion duration time but decreases with greater motion displacement. However, only for waves caused by downwards motion, does the wave period increase with raising bottom motion displacement surprisingly. More investigations are being carried out and will be reported shortly. In addition, due to the influence of reflection in this wave tank, an efficient long wave tank is under construction and will be used for further research.

ACKNOWLEDGMENTS

YSP acknowledges financial support from the Royal Society of Edinburgh through the Royal Society of Edinburgh and Scottish Government Personal Research Fellowship Co-Funded by the Marie-Curie Actions. This research is supported by the financial support from the Korea Institute of Marine Science and Technology Promotion [Reference No. 20140437].

References

Bogacki, P. and Shampine, L. (1989). A 3(2) pair of Runge-Kutta formulas. *Appl. Math. Lett.*, 2(4):321–325.

Chan, I.-C. and Liu, P. L.-F. (2012). On the runup of long waves on a plane beach. *J. Geophys. Res.*, 117(C08006).

Craig, W. (2006). Surface water waves and tsunamis. *J. Dyn. Differ. Equ.*, 18(3):525–549.

Dutykh, D. and Kalisch, H. (2013). Boussinesq modeling of surface waves due to underwater landslides. *Nonlinear Proc. Geoph.*, 20(3):267–285.

Dutykh, D., Katsaounis, T., and Mitsotakis, D. (2011). Finite volume schemes for dispersive wave propagation and runup. *J. Comput. Phys.*, 230(8):3035–3061.

Goring, D. G. (1978). *Tsunamis–the propagation of long waves onto a shelf*. PhD thesis, California Institute of Technology.

Hammack, J. L. (1973). A note on tsunamis: their generation and propagation in an ocean of uniform depth. *J. Fluid Mech.*, 60(04):769–799.

Harten, A. and Osher, S. (1987). Uniformly high-order accurate nonoscillatory schemes. i. *SIAM J. Numer. Anal.*, 24(2):279–309.

Kajiura, K. (1963). The leading wave of a tsunami. *B. Earthq. Res. I. Tokyo*, 41:535–571.

Keller, J. B. and Keller, H. B. (1964). Water wave run-up on a beach. Technical report, U.S. Department of the Navy.

Li, Y. and Raichlen, F. (2002). Non-breaking and breaking solitary wave run-up. *J. Fluid Mech.*, 456:295–318.

Liu, P. L.-F., Cho, Y.-S., Briggs, M. J., Kanoglu, U., and Synolakis, C. E. (1995). Runup of solitary waves on a circular island. *J. Fluid Mech.*, 302:259–285.

Liu, X.-D., Osher, S., and Chan, T. (1994). Weighted essentially non-oscillatory schemes. *J. Comput. Phys.*, 115(1):200¢212.

Madsen, P. A., Fuhrman, D. R., and Schäffer, H. A. (2008). On the solitary wave paradigm for tsunamis. *J. Geophys. Res.*, 113(C12012).

Madsen, P. A. and Schäffer, H. A. (2010). Analytical solutions for tsunami runup on a plane beach: single waves, N-waves and transient waves. *J. Fluid Mech.*, 645:27–57.

Mei, C. C. (1989). *The Applied Dynamics of Ocean Surface Waves*, volume 1. World scientific.

Peregrine, D. H. (1967). Long waves on a beach. *J. Fluid Mech.*, 27(04):815–827.

Shu, C.-W. (1998). Essentially non-oscillatory and weighted essentially non-oscillatory schemes for hyperbolic conservation laws. In Quarteroni, A., editor, *Advanced Numerical Approximation of Nonlinear Hyperbolic Equations*, volume 1697 of *Lecture Notes in Mathematics*, pages 325–432. Springer Berlin Heidelberg.

Sweby, P. K. (1984). High resolution schemes using flux limiters for hyperbolic conservation laws. *SIAM J. Numer. Anal.*, 21(5):995–1011.

Synolakis, C. E. (1987). The runup of solitary waves. *J. Fluid Mech.*, 185:523–545.

Tuck, E. O. and Hwang, L.-S. (1972). Long wave generation on a sloping beach. *J. Fluid Mech.*, 51(03):449–461.

Wu, T. Y.-T. (1987). Generation of upstream advancing solitons by moving disturbances. *J. Fluid Mech.*, 184:75–99.

Zelt, J. (1991). The run-up of nonbreaking and breaking solitary waves. *Coastal Eng.*, 15(3):205–246.